Interplay of the spin-density-wave state and magnetic field in the organic conductor α-(BEDT-TTF)$_2$KHg(SCN)$_4$

Takahiko Sasaki, Andrei G. Lebed,* and Tetsuo Fukase
Institute for Materials Research, Tohoku University, Katahira 2-1-1, Aoba-ku, Sendai 980-77, Japan

Naoki Toyota
Research Institute for Advanced Science and Technology, Osaka Prefecture University, Gakuen 1-2, Sakai 593, Japan
(Received 22 April 1996; revised manuscript received 29 July 1996)

Magnetic phase diagram of a quasi-two-dimensional organic conductor α-(BEDT-TTF)$_2$KHg(SCN)$_4$ is revisited from a viewpoint of magnetic torque measurements in high fields up to 30 T. A phase boundary that is interpreted as a metal-spin density wave (SDW) phase transition is found by using torque measurements. It is shown that this phase boundary is clearly distinguished from so-called kink transition of the magnetoresistance. We demonstrate that the transition temperature defined by the midpoint of the broad phase transition is almost independent on magnetic field up to 23 T. Onset temperature of the transition shifts from about 8 K at $H=0$ T to higher temperatures with increasing of a magnetic field, and tends to be saturated. The onset line of this transition follows well the theoretical expectation that SDW has to be stabilized by a magnetic field. This allows us to estimate such important band parameters of the quasi-one-dimensional section of the Fermi surface as an effective mass, $m^{1D}\simeq(0.5\pm0.1)m_0$, and an upper limit of an imperfect nesting bandwidth $t_c'\simeq(10\ \pm1)$ K. The other phase boundaries determined by the position of the kink and hysteresis properties of the magnetoresistance are interpreted as subphases inside the SDW phase. Inside the SDW phase, we find an additional phase boundary at the temperature-independent field of 23 T, which corresponds to the appearance of de Haas–van Alphen oscillations on a magnetic torque curve. At the 23 T boundary, both the effective mass, m^*, and the Dingle temperature, T_D, change their values from $m^*=(1.67\ \pm\ 0.05)\ m_0$ and $T_D=3.7$–4.0 K in low magnetic field region to $(1.95\ \pm\ 0.05)\ m_0$ and 2.5–2.8 K in high field region. The latter phenomenon is discussed in terms of a reconstruction of the Fermi surface due to the SDW formation. Hysteresis of the magnetoresistance observed in one of the subphases inside the SDW phase is studied in detail by measuring both the temperature and the magnetic field dependences. [S0163-1829(96)08342-7]

I. INTRODUCTION

An isostructural family of organic conductors α-(BEDT-TTF)$_2M$Hg(XCN)$_4$,[1–5] where BEDT-TTF is bis-(ethylenedithio)tetrathiafulvalen, has been the subject of intensive study due to a variety of the ground states.[6] While the superconductivity appears at about 1 K in α-(BEDT-TTF)$_2$NH$_4$Hg(SCN)$_4$,[7] the other salts with $M=$K or Tl, and $X=$Se remain to be a metal at least down to about 50 mK.[4,5] Much attention has been focused on the field-induced phase transitions in the salts with $M=$K, Tl or Rb, and $X=$S.[8–14] The ground state is thought to be commonly a spin-density-wave (SDW) condensation below $T_{\rm SDW}\simeq$ 8 K for the KHg(SCN)$_4$ salt, for example, where a shoulder-type resistance anomaly[15] and the anisotropic magnetic susceptibility typical for an antiferromagnetic ordering[16] appear. Below $T_{\rm SDW}$, the spontaneous moment of $3\times10^{-3}\mu_B$ is detected by zero field muon spin relaxation measurements.[17] Note that the SDW amplitude in our case is much smaller than that in (TMTSF)$_2$PF$_6$ ($\sim0.1\mu_B$),[18] where TMTSF is tetramethyltetraselenafulvalene. An apparent difference between BEDT-TTF and TMTSF salts is found in the Fermi surface (FS) topology. According to Mori's band structure calculation,[19] α-(BEDT-TTF)$_2M$Hg(SCN)$_4$ has both the quasi-two-dimensional (Q2D) and quasi-one-dimensional (Q1D) quasiparticle orbits. A couple of the Q1D FS sheets is likely to possess a nesting properties, and therefore the system is expected to be unstable against a periodic SDW modulation. On the contrary to TMTSF salts, in α-(BEDT-TTF)$_2M$Hg(SCN)$_4$, both Q1D and Q2D sections of FS coexist, that is a distinct feature of the latter material.

The reconstruction of the FS caused by the magnetic Brillouin zone due to the nesting, has been suggested so far by detailed studies of angle dependent magnetoresistance oscillations (ADMRO).[9,11,12,20,21] A number of magnetoresistance (MR) anomalies have been observed below $T_{\rm SDW}$. The MR rapidly increases with field up to its maximum value around 10 T. With further increase of the magnetic field, the MR continuously decreases down to so-called kink structure at 23 T and at higher field it increases again.[22] Hysteretic behavior is clearly observed for increasing and decreasing fields between about 8 and 23 T.[23,24] On the anomalous MR curve, complicated field-dependent spectrum of Shubnikov-de Haas oscillations are observed.[11,25] One of the most remarkable features of the MR is the observation of a sharp kink by Osada *et al.*[22] The kink field, H_a, shifts to lower field with increasing temperature and becomes zero at $T=T_{\rm SDW}$. The magnetic phase diagram that has been proposed is based on these magnetoresistance anomalies in magnetic fields perpendicular to the conducting a-c plane.[23,26] The field-induced transition in the present material has been considered to be different from that in the TMTSF

salts where an external field stabilizes the SDW state by improving the nesting condition due to the one dimensionalization of electron spectrum in a magnetic field.[27] To explain the experimental phase diagram of α-(BEDT-TTF)$_2M$Hg(SCN)$_4$, Osada *et al.*[28] have suggested that the magnetic breakdown between Q2D and Q1D sections of the FS could suppress the SDW transition. Kishigi and Machida[29] have obtained the similar results by calculating the free energy in the presence of a SDW state in a magnetic field. Thus a magnetic field has been considered to destabilize the SDW and the reentrance to the metallic state has been expected to occur at $H>H_a$. On the other hand, magnetic torque measurements by Christ *et al.*[30] demonstrate the existence of a hysteresis even above H_a. This result means that high-field phase above H_a is not a normal metallic state. Recently, we have reported about a possibility of the existence of a phase boundary (or crossover line) in the high-temperature normal metallic region. It was determined from a shallow minima in the temperature dependence of the resistivity in a magnetic field.[31] These recent experiments by Christ *et al.* and us demonstrate that the high-field phase at $H>H_a$ is different from the metallic phase above T_{SDW}.

In this paper, the magnetic torque measurements are presented to clarify the magnetic properties and the origin of the phase boundaries. The phase boundary is thermodynamically confirmed by the torque measurements. In addition, magnetoresistance measurements are extended to higher fields. The hysteresis phenomena of MR are studied in more detail. Finally, the magnetic phase diagram is revisited from the viewpoint of these measurements. Possible theoretical explanations for the transitions in fields are discussed.

II. EXPERIMENT

Single crystals of α-(BEDT-TTF)$_2$KHg(SCN)$_4$ were grown by the electro-oxidation method of BEDT-TTF in the distilled 1,1,2-trichloroethane with 10 volume % of the ethanol solution containing the purified electrolyte of KSCN, Hg(SCN)$_2$ and 18-crown-6 ether. The crystals having a typical size of a few mm$^2\times\sim$ 0.3 mm are grown on a platinum anode with the constant current of 0.5 μA. The well-developed facet is the crystallographic a-c plane.

The magnetic torque was measured with a capacitive cantilever beam torquemeter. The capacitor consists of a circular plate (3 mmϕ) as the moving electrode, which is suspended by a narrow beam (0.2 mm $\times$ 4 mm) made of thin beryllium copper (50 μm), and the sapphire plate with gold film sputtered as the ground plate. A single crystal of 2.92 mg is fixed on the moving plate with a small amount of grease. The capacitance measurements were done using a capacitance bridge (General Radio 1615A) and a lock-in-amplifier (PAR 124A). This torquemeter without the sample showed a small temperature and field dependence of the capacitance, which was reproducible both in the thermal and the field cycles. It may be due to a small amount of magnetic impurities in the beryllium copper used. No time dependence of the capacitance was observed. Therefore all of the data presented in this paper are corrected by subtracting the background measured in another run from the original data obtained. Resistivity measurements were done by a conventional four-terminal method using dc current of 100 μA in the a-c plane. The electrical terminals were made of the evaporated gold films, and gold wires (10 μmϕ) are glued onto the films with gold paint. The contact resistance was less than 10 Ω. Magnetic torque and resistivity measurements in field were carried out up to 14 T using the superconducting and 30 T hybrid magnets at High Field Laboratory, IMR, Tohoku University. The temperature in field was measured using Cernox thermometer (Lake Shore Cryotronics, Inc.) calibrated by a capacitance thermometer.

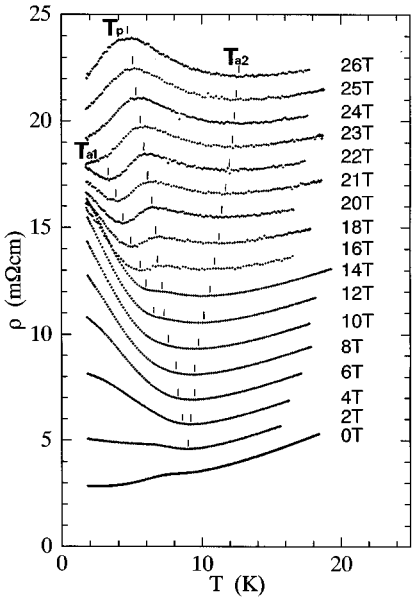

FIG. 1. Temperature dependence of the resistivity in fields perpendicular to the conductive a-c plane. The curves are shifted by 1 mΩ cm each from the data at $H=0$ T.

III. RESULTS AND DISCUSSION

A. Resistivity in magnetic field

Before proceeding to the magnetic torque measurements, we briefly review the temperature dependence of the resistivity obtained previously,[31] and present some new data up to 26 T.

Figure 1 shows the temperature dependence of the resistivity in a magnetic field normal to the conductive a-c plane. Each resistivity curve is shifted by 1 mΩ cm for clarity. A shoulder-type anomaly is observed around T_{SDW} = 8 K in $H=0$ T, which corresponds to the onset of the SDW transition expected from other measurements. With magnetic field, the magnetoresistance increases rapidly below the temperature of the resistivity minimum. We define this temperature as $T_{a1}^{\mathrm{MR}}(H)$ which corresponds to the kink transition and has been so far interpreted as an onset temperature for a density wave phase transition. Above 10 T, the enhancement of MR is gradually suppressed. Concurrently, $T_{a1}^{\mathrm{MR}}(H)$ shifts to lower temperatures and vanishes above $H=23$ T. It is noted that this behavior of $T_{a1}^{\mathrm{MR}}(H)$ is consistent with such experimental features as a rapid increase, a negative slope, and a kink in the isothermal MR. To summarize, the existence of a magnetic phase has been proposed so far on the basis of the field dependence of $T_{a1}^{\mathrm{MR}}(H)$. In our previous report,[31] we

mentioned about the shallow minimum which was attributed to a possible phase transition or a crossover between different magnetoresistance regions. The temperature $T_{a2}^{\mathrm{MR}}(H)$ defined by shallow minima as shown in Fig. 1 shifts to higher temperatures with increasing field, in contrast to the behavior of $T_{a1}^{\mathrm{MR}}(H)$. Both characteristic temperature, $T_{a1}^{\mathrm{MR}}(H)$ and $T_{a2}^{\mathrm{MR}}(H)$, approach to T_{SDW} when a magnetic field goes to zero. In the following sections, we show that such thermodynamic quantity as magnetic torque exhibits an enhancement due to the SDW formation below about 10 K in a magnetic field and defines a broad SDW phase transition. Although the shallow resistivity minima observed at $T_{a2}^{\mathrm{MR}}(H)$ do not indicate directly the phase transition, they can be attributed to the change of magnetoresistance on transition line, where the resistivity is increasing in a SDW phase. A maximum of magnetoresistance appears between the characteristic temperatures T_{a1}^{MR} and T_{a2}^{MR}. It defines some new crossover line $T_p(H)$.

B. Magnetic torque measurements

Magnetic torque is given by an expression of $\tau=\mathbf{M}\times\mathbf{H}$, where the magnetization is related to the susceptibility tensor $\hat{\chi}$ as follows, $\mathbf{M}=\hat{\chi}\mathbf{H}$. In the present material below T_{SDW}, there exists an anisotropic susceptibility component χ_A in addition to the isotropic one χ_{I}. In this case, the torque (per unit volume) is expressed as $\tau=H^2\chi_A\cos\theta\sin\theta$, where θ is the angle between a magnetic field and a direction normal to the a-c plane.

Figure 2(a) shows the temperature dependence of the torque at $\theta=17°$ in a magnetic field up to 27 T. The torque is increasing with increasing magnetic field. In the high-temperature region, it shows a little temperature dependence indicating by the solid lines. At lower temperatures, the magnetic torque increases below about 10 K, which is solely due to the increase of the anisotropic susceptibility component χ_A by the SDW transition. This transition is so broad as is observed in the static susceptibility measurements[16] that it is difficult to determine the certain transition temperature. To define onset temperature $T_{a2}^{\mathrm{t}}(H)$ of the SDW transition, a quantity $\Delta\tau$ [after subtracting a little temperature dependence which was extrapolated from a high-temperature region to lower temperature, see the solid lines in Fig. 2(a)] has been plotted in Fig. 2(b). The onset of the increase is defined as the temperature where $\Delta\tau$ exceeds the criterion level (10 dyn cm/g) that is determined by the resolution and stability in sweeping the temperature. We note that the large change in $\Delta\tau$ at low temperatures above 19 T is caused by de Haas-van Alphen (dHvA) effect considered in the next section. The definition of $T_{a2}^{\mathrm{t}}(H)$ is not influenced by this effect because the oscillation amplitude is negligibly small enough around 10 K. Uncertainty in the determination of the temperature is estimated to be about ± 0.5 K by taking the width of the criterion (± 50 %) into account. As shown in Figs. 2(a) and 2(b), $T_{a2}^{\mathrm{t}}(H)$ shifts to higher temperatures with increasing of a magnetic field and tends to be saturated. This onset temperature gives us a higher bound of the broad transition temperature. The other important points to be noted are that there are no magnetic torque anomaly at $T_{a1}^{\mathrm{MR}}(H)$ and that $T_{a2}^{\mathrm{t}}(H)$ disappears at $H>$ 23 T. The details of the magnetic phase diagram obtained on the basis of the behavior of $T_{a2}^{\mathrm{t}}(H)$ and $T_{a1}^{\mathrm{MR}}(H)$ are discussed in Sec. III E.

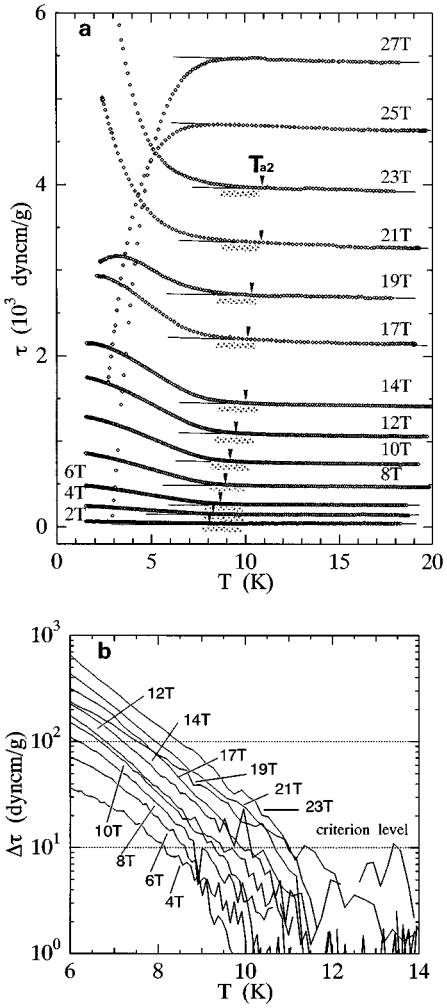

FIG. 2. (a) Temperature dependence of a magnetic torque in a constant magnetic field tilted by $\theta=17°$ from the direction normal to the conductive a-c plane. (b) Enhancement of the magnetic torque at low temperatures (after subtracting the high-temperature data extrapolated to low-temperature region). The transition line at $T_{a2}^{\mathrm{t}}(H)$ is determined by using the criterion level of 10 dyn cm/g.

Figure 3 demonstrates the behavior of torque scaled by H^2, $\tilde{\tau}\equiv\tau/H^2$. Above $T_{a2}^{\mathrm{t}}(H)$, $\tilde{\tau}$ is universal as a constant value of about 7.3 dyn cm/gT^2, which means that the anisotropic component χ_A is independent of the field. Below $T_{a2}^{\mathrm{t}}(H)$, on the other hand, χ_A is significantly dependent on temperature. Below 8 T, the torque is scaled as well as above T_{a2}^{t}, and χ_A increases with decreasing temperature. It has shown that the static spin susceptibility,[16] χ_{spin}, decreases below T_{SDW} in the case when field is applied parallel to the a-c plane, but remains almost constant at field normal to the plane. Therefore the magnetic easy axis of the antiferromagnetic ordering is expected to be in the a-c plane. The difference of the value of χ_{spin} between these two cases is $\Delta\chi_{\mathrm{spin}}=2-3\times10^{-4}$ emu/mole, which corresponds to the change of the anisotropy, $\Delta\chi_A$. The change in $\tilde{\tau}$ estimated from $\Delta\chi_{\mathrm{spin}}$ is about 4.7–7.2 dyn cm/gT^2. This value is in good agreement with the observed change of the torque which is about 6.8 dyn cm/gT^2. Above 8 T, the torque be-

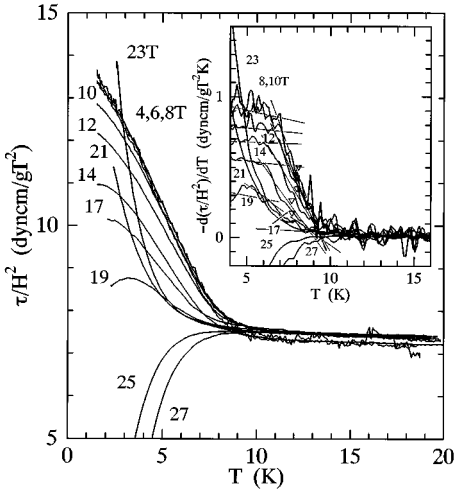

FIG. 3. Temperature dependence of the magnetic torque divided by the field squared. Above T_{a2}^{t}, the torque is scaled at the constant value of about 7.3 dyn cm/gT^2. The inset shows the temperature derivative of $\tilde{\tau}$. A midpoint of the broad transition is marked by an open triangle.

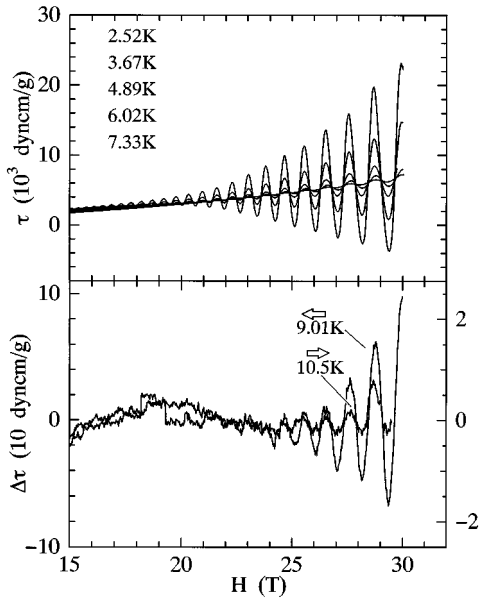

FIG. 4. Field dependence of the magnetic torque and de Haas-van Alphen oscillations. In the lower panel, background subtraction is applied to the data.

gins to deviate downward from the scaled curve. This deviation corresponds to the decrease of χ_A, suggesting that the moment of the SDW might become smaller or cant toward a magnetic field direction. The field at which the anisotropy starts to change with field is much higher than that in the SDW states in TMTSF salts. For example, $(TMTSF)_2AsF_6$ with $T_{SDW} = 12$ K shows a spin-flop transition at $H = 0.45$ T.[32] The reason for this difference between two families of organic conductors is not clear yet.

The inset in Fig. 3 shows the temperature derivative of $\tilde{\tau}$ to demonstrate the broad SDW transition. The width of the broad transition is estimated to be about $2 \sim 3$ K around 8 K. The transition temperature is defined by a midpoint of the slope in the transition region, which is marked by an open triangle. We found that a midpoint of this broad transition seems to be almost independent on magnetic field. This field dependence is quite different with $T_{a1}^{MR}(H)$ defined from the kink structure of MR.

It is shown that the field region between 8 and 23 T, where χ_A changes with magnetic field, corresponds to a wide hysteresis of MR observed before. This means that the hysteresis of MR closely relates to the field dependence of the magnetic properties as it is seen from χ_A behavior. Nevertheless, no hysteresis is observed both in the field and temperature dependences of the torque, which is in disaccordance with the large hysteresis observed above 23 T and below 1 K by Christ *et al.*[30] As it is pointed out in the next section, our measurements of the field dependence of the torque are available for $T > 2.52$ K, which might be the reason for nonobservation of hysteresis phenomenon at $H > 23$ T. The detail of the hysteresis phenomenon is discussed in Sec. III D.

C. de Haas-van Alphen effect

In Fig. 4, we show dHvA signals on a magnetic torque curve at $\theta = 17°$. The data at 9.01 and 10.5 K obtained after subtracting the monotonic background from the original ones show the quantum magnetic oscillations visible even at these high temperatures. The characteristic splitting of dHvA signal, which has been revealed below H_a, is not observed at temperatures above 2.52 K. The oscillation frequency F is found to be 704 ± 5 T both above and below H_a. The observed frequency is in good agreement with the previous SdH results for the angle dependence of F, $F = 670/\cos(17°)$ (T) $\simeq 700$ T, which is a characteristic of a cylindrical FS. The organic conductor under consideration is known to have both Q2D and Q1D FS's above the SDW transition. In the perfect 2D case, it is known that the field dependence of the oscillation amplitude is different from the conventional 3D Lifshitz-Kosevich (LK) formula. The reason is that the nonoscillatory part of the density of states is essentially independent of energy, ε, in the 2D case, in contrast to 3D case where it is increasing as $\varepsilon^{1/2}$ (Refs. 33 and 34). Thus the additional factor of $(\mu/\hbar\omega_c)^{1/2} \propto H^{-1/2}$ is present in the 3D-LK expression for magnitude of SdH or dHvA oscillations, where $\mu = m^*/m_0$ is the effective mass ratio to bare electron mass, m_0, and $\omega_c = eH/m^*c$ is the cyclotron frequency. Recently, the application of the 2D formulas to the isostructural organic conductor α-$(BEDT\text{-}TTF)_2KHg(SeCN)_4$ was tested.[4] According to Ref. 4, the conventional 3D-LK formulas can reproduce the results better than the corresponding 2D expression. In this paper, both the conventional 3D-LK expression and the 2D expression are used to analyze the dHvA oscillations and to evaluate Dingle temperature. It is noted that, in general, the procedure to determine the effective mass is independent on 2D or 3D formulas.

The first harmonics of the oscillatory part of the torque (3D case) is given by[35]

$$\tau_{osc} = -\frac{1}{F}\frac{dF}{d\theta} M_{osc} H, \tag{1}$$

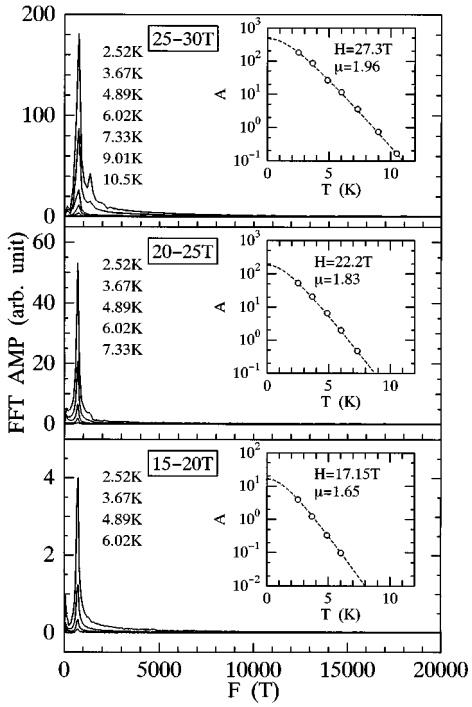

FIG. 5. Fourier transformations of the data in Fig. 4 carried out in the field range of 25–30, 20–25, and 15–20 T. The inset shows the temperature dependence of the Fourier amplitude (A) at the fundamental frequency of 704 T. The broken curve shows the fitting one to Eq. (2) using the parameters in each panel.

$$M_{\rm osc} \propto TFH^{-1/2} \frac{\exp(-\lambda \mu T_D/H)}{\sinh(\lambda \mu T/H)} \cos(\pi g \mu/2) \times \sin(2\pi F/H + \phi), \quad (2)$$

where $\lambda \equiv 2\pi^2 m_0 c k_B/e\hbar = 14.69$ T/K, c is the light velocity, k_B the Boltzmann's constant, $\hbar$ the Planck's constant, g the so-called electron g factor ($g \simeq 2$), and T_D is the Dingle temperature. In the 2D case, the exponent of the magnetic field should be changed from $-1/2$ into $1/2$ in Eq. (2). The effective mass is determined by fitting the experimental dHvA oscillation amplitude to Eqs. (1) and (2). The amplitudes of the oscillations were determined by two ways, application of Fourier analysis for 15T$<H<$20 T, 20 T $<H<$25 T, and 25 T$<H<$30 T and measuring the peak-to-peak amplitudes for each oscillation. Figure 5 shows the frequency spectra obtained by fast Fourier transformation (FFT). The second harmonics is not so strong at these temperatures that the contribution of the higher harmonics can be neglected in our analysis. The insets show the temperature dependence of the first harmonic amplitude which corresponds to the fundamental frequency of 704 T as previously described. The broken lines in each inset are the fitting curves obtained from Eqs. (1) and (2) with the parameters of $\mu = 1.96$ at $H = 27.3$ T, 1.83 at 22.2 T, and 1.65 at 17.15 T. These values of magnetic field are determined as the center in the reciprocal-field space for each field range. The obtained effective mass increases with increasing field. Concerning the effective mass of this material, there have been reported the different value in high magnetic field.[11,14,24,30,36] The effective masses determined from the amplitude of the FFT spectra are shown by the filled circles in Fig. 6. In addition, the open circles denote the mass determined from the measuring of the peak-to-peak amplitude of each oscillation. The values estimated by these two methods are in good agreement with each other, since the higher-order harmonics are too weak in the oscillations measured under the present experimental conditions. The effective mass clearly demonstrates a magnetic field dependence. It is almost constant below 20 T ($\mu \simeq 1.67 \pm 0.05$ on the average) and above 25 T ($\mu \simeq 1.95 \pm 0.05$). Between these crossover, there appears a pronounced change of the effective mass at about 23 T. In our previous measurements[36] up to 25 T, no field-dependent mass was reported. This contradiction is due to the different experimental conditions of the field and temperature regions analyzed. The present results are in good agreement with those obtained by Christ *et al.*[30] and Pratt *et al.*[24] including the quoted value of effective masses. In addition, Harrison *et al.* reported similar change of the mass from $\mu \simeq 1.5$ (low fields) to $\simeq 2.7$ (high fields), using the inductive method in a pulsed-field experiment.[14] The reason for the different values of the effective mass obtained at high magnetic fields is still unclear. Note that the determination of the effective mass may somewhat depend on the experimental method.

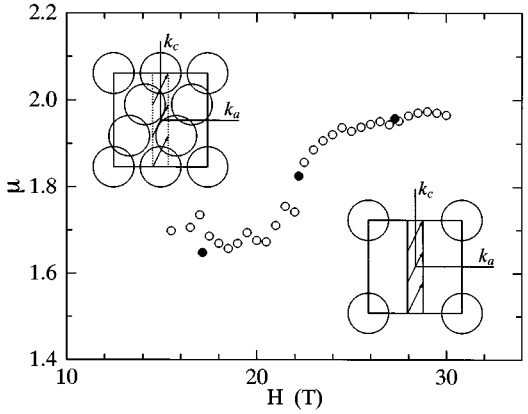

FIG. 6. The effective mass plotted as a function of field. The mass indicated by the filled and the open circles are derived from the temperature dependence of the Fourier amplitude at the fundamental frequency and the peak-to-peak amplitude of the oscillations, respectively. The schematic Fermi surface is shown in the inset: (a) Fermi surface calculated by the tight-binding approximation in Ref. 19, which is prior to the SDW formation. The arrows are the possible nesting vector expected from the ADMRO measurements. (b) The multiconnected Fermi surface reconstructed by nesting the open part due to the SDW formation after Ref. 20.

Figure 7 shows Dingle plots at different temperatures obtained by using the 3D (upper panel) and the 2D-LK (lower panel) expressions with the effective mass obtained as a function of magnetic field (see Fig. 6). The change of the slope are clearly seen around 23 T in both cases. According to LK formulation, the slope is equal to $-\lambda \mu T_D$. Two different Dingle temperatures are obtained from the slope of the fitting lines: $T_D = 3.7$ K (4.0 K) at low fields and $T_D = 2.5$ K (2.8 K) at high fields in the 3D (2D) case. Comparing the two cases, it is hard to say which case does reproduce the experimental data better at these temperatures and magnetic fields. Deviations from the conventional 3D-LK expression and tendency to 2D behavior should be significant at lower

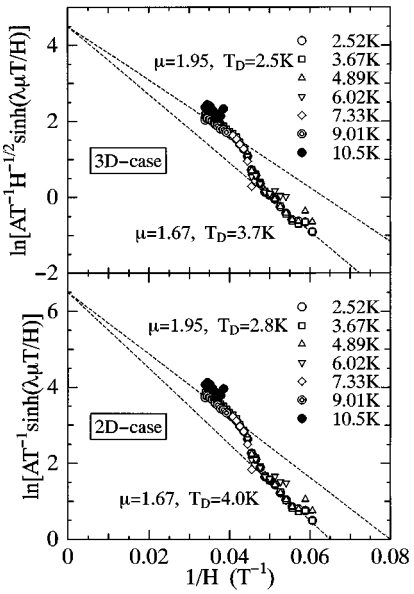

FIG. 7. Dingle plots for the peak-to-peak amplitude of the de Haas-van Alphen oscillations obtained using the 3D (upper panel) and the 2D-LK (lower panel) expressions.

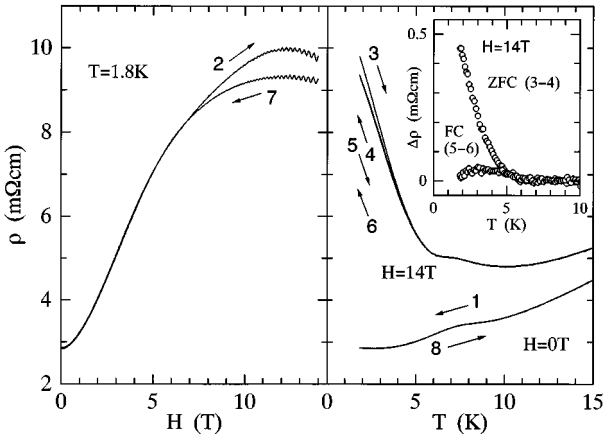

FIG. 8. Temperature and field dependence of the resistivity. The number noted on each curve indicates the order of the measurement. The inset in the right panel shows the difference of the resistivity between routes (3) and (4) (ZFC) and between (5) and (6) (FC).

temperature and higher magnetic field in Q2D organic conductor α-(BEDT-TTF)$_2$KHg(SCN)$_4$. The general features of the Dingle plot, however, does not change in either 3D or 2D case except for the small change (about 0.3 K) in the evaluated T_D. Our previous results[36] up to 23 T shows only the increase of T_D. The data clearly indicate the transition between high-T_D and low-T_D states around 23 T, which confirms recent results.[14,30] It should be noted that the transition field does not show any temperature dependence at least up to 7.33 K. As reported so far,[14,30,36] the change in the slope has been related to H_a or T_{a1}, where the kink of MR appears. Our findings show that such a correspondence is not correct except at $T \simeq 0$ K. Thus we conclude that the transition between the small-μ, high-T_D state, and large-μ, low-T_D one occurs at the temperature independent field of 23 T.

Two possible mechanisms for the change of T_D are discussed as follows. The magnetic oscillation of the α orbit with $F(\theta=0°)=670$ T and 704 T at $\theta=17°$ in the SDW state has been considered to be caused by the magnetic breakdown (MB) between the multiconnected orbits, resulting from the reconstruction of the Brillouin zone by the SDW nesting vector. The schematic reconstructed FS is shown in the inset of Fig. 7, which is originally proposed by Kartsovnik *et al.*[20] This model has been supported by ADMRO experiments by several groups (Refs. 9, 11, 12, 20, and 21), and is consistent with small FS pockets observed in low fields.[13] In this case, the additional damping factor appears in the field dependence of the oscillation amplitude. The factor $R_{\mathrm{MB}}=\exp(-2H_{\mathrm{MB}}/H)$ must be added to Eq. (2) in this case of the four-breakdown points, where H_{MB} is a characteristic field of MB. Thus, the Dingle temperature of the MB orbit is described as $T_D^{\mathrm{obs}}=T_D+T_D^{\mathrm{MB}}$ where $T_D^{\mathrm{MB}}=2H_{\mathrm{MB}}/\lambda\mu$. From the difference of the Dingle temperatures, H_{MB} is estimated as 14.7 T. This value is somewhat higher than the field at which the oscillation is observed. In the case of κ-(BEDT-TTF)$_2$Cu(NCS)$_2$, the magnetic breakdown oscillations could be observed above H_{MB} of about 16 T.[37,38] The difference between these two cases may be ascribed to the effective mass of each MB orbit. The mass in κ-(BEDT-TTF)$_2$Cu(NCS)$_2$ is about four times as heavy as that of the present salt. The small effective mass in the material under consideration is the reason why the oscillations are observed in lower fields.

Another explanation for the change of T_D is that the formation of the SDW may induce an excess scattering on the carriers as discussed by Harrison *et al.*[14] Although it has not been unclear how the SDW introduces a disorder into the system, the domain boundary assumed for the mixture of the SDW and normal metal states proposed by Athas *et al.*[39] might be the origin of the disorder.

In any case, the temperature-independent transition at 23 T, indicating the reconstruction of the Brillouin zone due to the SDW formation, suggests that the SDW below 23 T survives up to about 10 K. This result also strongly supports that T_{a2} determined in the previous section is the transition temperature of the SDW.

D. Hysteresis of magnetoresistance

Notable hysteresis of MR is one of the characteristic features in the SDW phase. The hysteresis of the isothermal MR has been observed in fairly wide field range between 8 and 23 T. The MR for decreasing field takes always lower value than that for increasing field. In order to observe the complete hysteresis, it is necessary to sweep the field fully between 0 and above H_a. Incomplete scan of the field has produced the local hysteresis around H_a. In this way, such hysteresis may depend on the condition and/or the history of the temperature and the field.

Figure 8 shows the temperature and the field dependence of the resistivity taking the history into account. The sweep rate of the temperature and the field are 0.4 K/min and 0.3 T/min, respectively, for all the measurements. The numbers noted on each curve indicate the order of the measurements: (1) the sample is cooled in zero field down to 1.8 K, (2) then the magnetic field is sweeping up to 14 T as shown in the

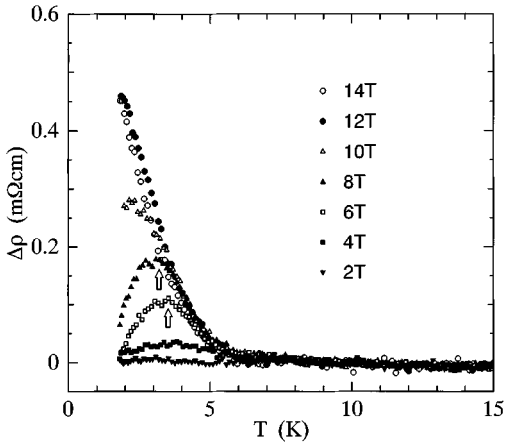

FIG. 9. The difference of the resistivity between routes (3) and (4) at each field. The arrows indicate the points where the difference starts decrease.

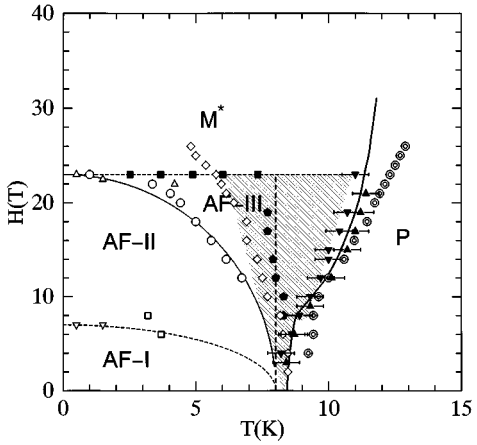

FIG. 10. Magnetic phase diagram of α-(BEDT-TTF)$_2$KHg(SCN)$_4$. The marks and the lines are referred to the text.

figure, (3) it is warmed up to 18 K at 14 T and (4) cooled down to 1.8 K. In this process, T_{a1}^{MR} and T_{a2}^{MR} are clearly observed. It is noted that the resistivity in the route (4) is smaller than that in (3) below T_{a1}^{MR}. After cooling in field, the same process of (5) and (6) is done. The resistivities in (4), (5), and (6) take the same value. The inset shows the difference of the resistivity between the route (3) and (4) (ZFC) and between (5) and (6) (FC). This result shows that the resistivity only after cooled in zero field takes high value in the hysteresis. After (6), the field decreases at 1.8 K (7). Below about 7 T, the MR becomes reversible. There is no difference of the resistivity in zero field after the measurements (8). No time relaxation of MR is observed for 6 hours at 1.8 K and 14 T after the process of (2).

Figure 9 shows the difference of the resistivities between routes (3) and (4) at each constant field where the maximum field is being reached in the process of (2) after (1). At 6 and 8 T, the difference becomes small below the temperature marked by the arrows. These points divide the magnetic field-temperature phase diagram into two parts below T_{a1}^{MR}, i.e., the phase with the reversible and irreversible resistivity observed for the temperature and the field.

E. Magnetic phase diagram

Figure 10 shows the magnetic phase diagram based on the MR, torque measurements and dHvA oscillations described above. The meaning of the marks in Fig. 10 are the open circles and triangles for T_{a1}^{MR}, the double circles for T_{a2}^{MR}, the open diamonds for T_p, the filled reverse triangles for T_{a2}^{t} at $\theta=17°$, the filled triangles for T_{a2}^{t} at $\theta=38°$, the filled pentagons for a midpoint of the broad transition observed by the magnetic torque, the open reverse triangles for the irreversibility line for sweeping field, the open squares for the points indicated in Fig. 9 and the filled squares for the change of μ and T_D in the dHvA oscillations. The hatched region represents a broad metal-SDW transition. The thin broken curves are guides for the eye. The thin solid curve is determined from fitting T_{a1}^{MR} to an empirical formula,

$$T_{a1}^{\mathrm{fit}}(H)=T_{\mathrm{SDW}}^{\mathrm{fit1}}[1-(H/H_{\mathrm{SDW}}^{\mathrm{fit}\,1})^2]^{1/2}, \qquad (3)$$

where $T_{\mathrm{SDW}}^{\mathrm{fit1}}$ and $H_{\mathrm{SDW}}^{\mathrm{fit1}}$ are the fitting parameters. Note that Eq. (3) is analogous to the one describing the Pauli paramagnetic effect on a superconductor. The fitting parameters are obtained to be $T_{\mathrm{SDW}}^{\mathrm{fit1}}=8$ K and $H_{\mathrm{SDW}}^{\mathrm{fit1}}=23$ T.

We consider the phase transition determined by the magnetic torque and resultant shallow minimum of MR as a firm confirmation of the existence of a metal-SDW phase transition. A shallow minimum observed at $T_{a2}^{\mathrm{MR}}(H)$ in the resistivity results from the crossover between the different magnetoresistance behavior in the normal metal and the SDW phases. The thick curve shows theoretical results for the field response of SDW, which is fitted to $T_{a2}^{\mathrm{t}}(H)$. The detail is described in Sec. III F. The three main phases are recognized as follows: the first is a paramagnetic normal metallic state denoted by P, the second is antiferromagnetic SDW phases by AF, and the third is some unknown metallic phase by M^* which is different from the simple P state. In the AF phase, there are at least three subphases as I, II, and III. The AF and M^* phases are summarized as follows. The AF phases are characterized by the presence of the anisotropic component of the susceptibility due to the SDW. In the AF-I phase, the spontaneous antiferromagnetic moment due to the SDW may lie in the plane. The difference of the anisotropic component of the susceptibility in field parallel and perpendicular to the plane does not change with field, and the MR shows reversible rapid increase with field. The boundary between the AF-II and the AF-III, which is clearly characterized by MR, is not recognized well from the magnetic torque measurements. The anisotropic component of the susceptibility decreases with increasing field as shown in Fig. 3. The irreversible MR is observed in the AF-II, only when the field and temperature are scanned through the AF-II between the AF-I and the AF-III or M^*. In the highest field phase M^* where dHvA oscillations are predominant, the torque looks like that in the P phase, and the anisotropic component of the susceptibility should be quite small if any, while the MR shows quite different behavior from that in the P phase. It is hard to conclude from the present measurements whether the M^* phase still remains magnetic or not. The reason is that the torque could not detect any change if the finite moment exists there and turns easily toward the field direction.

F. SDW: theory versus experiment

The goal of this section is to give a quantitative description of the onset temperature of the metal-SDW transition boundary derived from the torque measurements. This allows us to estimate such important parameters of Q1D sections of the FS as effective mass, m^{1D}, and so-called imperfect nesting term, t_c'. Since while fitting of the theoretical equations obtained in this section to experimental data, the onset temperature, $T_{a2}^{t}(H)$, is used, the obtained value of t_c' should be interpreted as a high limit of imperfect nesting bandwidth. We recall that in the case of perfect nesting ($t_c'=0$) the metal-SDW transition does not show any field dependence.

From papers on SDW formations in a magnetic field,[40–42] it is known that a magnetic field improves the nesting properties of Q1D sheets of FS and leads to the creation of SDW in $(TMTSF)_2ClO_4$, $(TMTSF)_2ReO_4$, and some others Q1D compounds. In $(TMTSF)_2PF_6$ salt, where SDW is stable at $H=0$, it was shown both theoretically[43] and experimentally[44] that a magnetic field slightly increases T_{SDW} being H^2 dependent at low enough fields:

$$T_{SDW}(H)-T_{SDW}(0)=\frac{\omega_c^2}{T_{SDW}(0)}F\left(\frac{t_c'}{T_{SDW}(0)}\right), \qquad (4)$$

where F is a dimensionless function,[43] $\omega_c=eHv_F^{1D}d_c/c$ is a characteristic frequency of an electron motion along open FS's, d_c is a lattice constant along the c^* direction, c is the velocity of light. Thus, from this point of view, our observation of increasing $T_{a2}^{t}(H)$ with magnetic field in α-$(BEDT\text{-}TTF)_2KHg(SCN)_4$ is qualitatively consistent with the interpretation of low-temperature phase as SDW one.

Nevertheless, there are two main differences between SDW's in $(TMTSF)_2PF_6$ and α-$(BEDT\text{-}TTF)_2KHg(SCN)_4$. On the contrary to $(TMTSF)_2PF_6$, α-$(BEDT\text{-}TTF)_2KHg(SCN)_4$ demonstrates more pronounced increase in $T_{SDW}(H)=T_{a2}^{t}(H)$ which obeys H^2 law only at $H<8$ T and tends to saturate at higher magnetic fields (see Fig. 10). The other obvious difference is the coexistence of both open and closed quasiparticle orbits in BEDT-TTF conductors. This coexistence of Q1D and Q2D sections of the FS results in two complications. According to Kartsovnik description,[20] we have to consider a reconstruction of Q2D orbits below the SDW transition, where Q1D orbits disappear. In addition, the above-mentioned coexistence cannot give us an opportunity to determine the effective mass, m^{1D}, by using the available data on the specific heat and/or magnetic susceptibility in a paramagnetic metal phase as it was done for $(TMTSF)_2PF_6$ in Ref. 44.

Therefore, we present some more general description of SDW in a magnetic field than it was done in Ref. 43, in order to derive all Q1D band parameters, m^{1D}, v_F^{1D} and t_c' directly from the comparison of the theoretical results with the experimental T_{a2}^{t} curve. We start from the simplified electron spectrum that is usually considered to describe Q1D band:[27]

$$\epsilon(\vec{p})=\pm v_F^{1D}(p_a\mp p_F)+2t_c\cos(p_cd_c\mp\alpha)+2t_c'\cos(2p_cd_c\mp 2\alpha), \qquad (5)$$

where the Fermi velocity, v_F^{1D} corresponds to a free 1D electron motion in the direction perpendicular to the slightly modulated sheets of FS, t_c stands for the main contribution from the corrugations of Q1D FS, which provides an ideal nesting condition, and the term with $t_c'\ll t_c$ is responsible for small deviations from ideal nesting.

Note that the closed sections of the FS give relatively small contribution to Peierls instability and can be neglected in calculating $T_{SDW}(H)$. As shown in Sec. III B at magnetic fields $H>8$ T, electron spins follow the direction of a field that give us an opportunity to consider the SDW response on a magnetic field in the framework of the standard model.[40–42] Performing calculations analogous to Ref. 40 we obtain the following expression for $T_{SDW}(H)$:

$$\ln\left(\frac{T_{SDW}(H)}{T_{SDW}(0)}\right)=\int_0^\infty\frac{dx}{\sinh(x)}\left\{J_0\left[\frac{4t_c'}{\omega_c}\sin\left(\frac{\omega_c x}{2\pi T_{SDW}(H)}\right)\right]-J_0\left(\frac{2t_c'x}{\pi T_{SDW}(0)}\right)\right\}. \qquad (6)$$

Note that Eq. (6) contains two unknown parameters t_c' and v_F^{1D} Due to the existence of a characteristic inflection point on the experimental curve $T_{a2}^{t}(H)$, it is possible to determine both of them by numerical fitting of Eq. (6). After this procedure, we get the results: $v_F^{1D}\simeq(1.7\pm0.2)\times10^7$ cm/sec, $m^{1D}\simeq(0.5\pm0.1)m_0$, and $t_c'\simeq(10\pm1)$ K. At this point, it is useful to compare the band parameters of Q1D orbits estimated by us with the results of band structure calculations (see Mori *et al.*, Ref. 19). The above-obtained value, $m^{1D}=0.5m_0$, is almost two times larger than the calculated one, $m^{1D}=0.3-0.4m_0$. Probably, this difference is a manifestation of an importance of electron-electron and/or electron-phonon interactions in α-$(BEDT\text{-}TTF)_2KHg(SCN)_4$. Then, by analyzing the curve $T_{a2}^{t}(H)$, we can estimate a deviation from the nesting properties of Q1D sections of FS as $t_c'=$ 10 K. Since the estimated value of t_c' is small enough, it confirms both Mori's calculations[19] and so-called Kartsovnik description.[20]

By using the relationship between $T_{SDW}(0)$ and saturation temperature $T_{SDW}(\infty)$:

$$\ln\left(\frac{T_{SDW}(\infty)}{T_{SDW}(0)}\right)=\int_0^\infty\frac{dx}{\sinh(x)}\left[1-J_0\left(\frac{2t_c'x}{\pi T_{SDW}(0)}\right)\right], \qquad (7)$$

we obtain for $T_{SDW}(\infty)$ the value of (12.5 ± 1) K.

It is worth to derive some analytical expressions for the $T_{SDW}(H)$ that are applicable both for α-$(BEDT\text{-}TTF)_2KHg(SCN)_4$ and $(TMTSF)_2PF_6$ salts. In addition to known Eq. (4) (Ref. 43) [which is valid only for small magnetic fields, $\omega_c\ll T_{SDW}(0)$, and does not show any saturation], we present some more common analytical formulas:

$$\ln\left(\frac{T_{\mathrm{SDW}}(\infty)}{T_{\mathrm{SDW}}(H)}\right)=\left(\frac{t_c'}{\omega_c}\right)^2\left[\psi\left(\frac{1}{2}-i\frac{\omega_c}{2\pi T_{\mathrm{SDW}}(H)}\right)+\psi\left(\frac{1}{2}+i\frac{\omega_c}{2\pi T_{\mathrm{SDW}}(H)}\right)-2\psi\left(\frac{1}{2}\right)\right], \tag{8}$$

where ψ is the so-called psi function (see, for example, Ref. 45):

$$\psi(x)=-C-\sum_{k=0}^{\infty}\left(\frac{1}{k+x}-\frac{1}{1+k}\right), \tag{9}$$

and C is Euler's constant. Note that Eq. (8) is applicable for the arbitrary magnetic fields in the experimentally interesting case when $t_c'\sim T_{\mathrm{SDW}}(0)$. It is important that, for strong and moderate magnetic fields [when $\omega_c/\pi T_{\mathrm{SDW}}(0)\geqslant 1$], Eq. (8) is significantly simplified:

$$\ln\left(\frac{T_{\mathrm{SDW}}(\infty)}{T_{\mathrm{SDW}}(H)}\right)=\frac{4t_c'^2}{[\pi T_{\mathrm{SDW}}(H)]^2+\omega_c^2}. \tag{10}$$

Using Eqs. (4) and (10), we present the theoretical curve by a thick solid line. The theoretical curve can reproduce $T_{a2}^{\mathrm{t}}(H)$ well with use of reasonable parameters of $m^{1\mathrm{D}}$ and t_c'

IV. CONCLUSION

In this paper, we have reported both the temperature and the magnetic field dependence of MR and torque in the SDW phase of the organic conductor α-(BEDT-TTF)$_2$KHg(SCN)$_4$. The metal-SDW transition is thermodynamically determined by using magnetic torque measurements in the high-field region. This phase boundary is also characterized by shallow minima of MR around $T\simeq 10$ K. The metal-SDW transition is so broad that it is difficult to define unique temperature of the phase transition. Although the increase in onset temperature with increasing magnetic field is in agreement with theoretical description, the temperature defined by the midpoint of the broad transition seems to be independent of magnetic field.

Below, we summarize some unsolved problems regarding the magnetic phase diagram of α-(BEDT-TTF)$_2$KHg(SCN)$_4$: (i) The nature of $T_{a1}^{\mathrm{MR}}(H)$ line still remains unclear. Moreover the transition at $T_{a1}^{\mathrm{MR}}(H)$ has been observed only in transport properties such as MR, but not in torque. (ii) Are the magnetic properties in the M^* phase still AF-like or not? Note that dHvA and ADMRO effects demonstrate that the reconstruction of FS is removed there. (iii) It is important to clarify the origin of the crossover line $T_p(H)$ since this line crosses the boundary between the AF-III and M^* phases. We speculate that it is somehow related to the MB phenomenon across some gap which is opened due to the appearance of SDW potential below $T_{\mathrm{SDW}}(H)$.[46] (iv) The origin of hysteresis observed in MR only inside the AF-II phase is not clear. According to the present study, the possibility for the extrinsic origin of the hysteresis due to the contamination of the metallic domain by fast cooling the sample is excluded.

ACKNOWLEDGMENTS

This work was carried out at High Field Laboratory for Superconducting Materials, IMR, Tohoku University and partially supported by a Grant-in-Aid for Scientific Research on the priority area, Novel Electronic States in Molecular Conductors, from the Ministry of Education, Science, and Culture of Japan. Professor M. Motokawa is appreciated for his encouragement. The authors would like to thank Dr. M. V. Kartsovnik, Dr. W. Biberacher, and Professor K. Machida for stimulating discussions.

*On leave from L. D. Landau Institute for Theoretical Physics, Russian Academy of Science, Moscow, Russia.

[1] M. Oshima, H. Mori, G. Saito, and K. Oshima, Chem. Lett. **1989**, 1159 (1989).

[2] H. Mori, S. Tanaka, K. Oshima, M. Oshima, and G. Saito, Solid State Commun. **74**, 1261 (1990).

[3] N. D. Kushch, L. I. Buravov, M. V. Kartsovnik, V. N. Laukhin, S. I. Pesotskii, R. P. Shibaeva, L. P. Rozenberg, E. B. Yagbuskii, and A. V. Zvarikina, Synth. Met. **46**, 271 (1992).

[4] T. Sasaki, H. Ozawa, H. Mori, S. Tanaka, T. Fukase, and N. Toyota, J. Phys. Soc. Jpn. **65**, 213 (1996).

[5] L. I. Buravov, N. D. Kushch, V. N. Laukhin, A. G. Khomenko, E. B. Yagubskii, M. V. Kartsovnik, A. E. Kovalev, L. P. Rozenberg, R. P. Shibaeva, M. A. Tanatar, V. S. Yefanov, V. V. Dyakin, and V. A. Bondarenko, J. Phys. (France) I **4**, 441 (1994).

[6] For a recent review, see *Proceedings of the International Conference on Science and Technology of Synthetic Metals*, Seoul, Korea, 1994 [Synth. Met. **69-71** (1995)].

[7] H. H. Wang, K. D. Carlson, U. Geiser, W. K. Kwok, M. D. Vashon, J. E. Thompson, N. F. Larsen, G. D. McCabe, R. S. Hulscher, and J. M. Williams, Physica C **166**, 57 (1990).

[8] On this subject, there have been many articles published so far. Thus the readers are referred to Refs. 9–14, containing the comprehensive references for the earlier works.

[9] T. Sasaki and N. Toyota, Phys. Rev. B **49**, 10 120 (1994).

[10] J. S. Brooks, X. Chen, S. J. Klepper, S. Valfells, G. J. Athas, H. Anzai, and C. C. Agosta, Phys. Rev. B **52**, 14 457 (1995).

[11] J. Caulfield, S. J. Blundell, M. S. L. du Croo de Jongh, P. T. J. Hendrics, J. Singleton, M. Doporto, F. L. Pratt, A. House, J. A. A. J. Perenboom, W. Hayes, M. Kurmoo, and P. Day, Phys. Rev. B **51**, 8325 (1995).

[12] M. V. Kartsovnik, A. E. Kovalev, V. N. Laukhin, I. F. Schegolev, H. Ito, T. Ishiguro, N. D. Kushch, H. Mori, and G. Saito, Synth. Met. **70**, 811 (1995).

[13] S. Uji, H. Aoki, M. Tokumoto, T. Kinoshita, N. Kinoshita. Y. Tanaka, and H. Anzai, Phys. Rev. B **49**, 732 (1994).

[14] N. Harrison, A. House, I. Deckers, J. Caulfield, J. Singleton, F. Herlach, W. Hayes, M. Kurmoo, and P. Day, Phys. Rev. B **52**, 5584 (1995).

[15] T. Sasaki, N. Toyota, M. Tokumoto, N. Kinoshita, and H. Anzai, Solid State Commun. **75**, 93 (1990).

[16] T. Sasaki, H. Sato, and N. Toyota, Synth. Met. **41-43**, 2211 (1991).

[17] F. L. Pratt, T. Sasaki, and N. Toyota, Phys. Rev. Lett. **74**, 3892 (1995).

[18] L. P. Le, A. Keren, G. M. Luke, B. J. Sternlieb, W. D. Wu, Y. J.

Uemura, J. H. Upsani, L. Y. Chiang, W. Kang, P. M. Chaikin, T. Csiba, and G. Grüner, Phys. Rev. B **48**, 7284 (1993).
[19] H. Mori, S. Tanaka, M. Oshima, G. Saito, T. Mori, Y. Maruyama, and H. Inokuchi, Bull. Chem. Soc. Jpn. **63**, 2183 (1990).
[20] M. V. Kartsovnik, A. E. Kovalev, and Kushch, J. Phys. (France) I **3**, 1187 (1993); M. V. Kartsovnik, A. E. Kovalev, V. N. Laukhin, and S. I. Pesotskii, J. Phys. (France) I **2**, 223 (1992).
[21] Y. Iye, R. Yagi, N. Hanasaki, S. Kagishima, H. Mori, H. Fujimoto, and G. Saito, J. Phys. Soc. Jpn. **63**, 674 (1994).
[22] T. Osada, R. Yagi, A. Kawasumi, S. Kagoshima, N. Miura, M. Oshima, and G. Saito, Phys. Rev. B **41**, 5428 (1990).
[23] T. Sasaki and N. Toyota, Solid State Commun. **82**, 447 (1992).
[24] F. L. Pratt, J. Singleton, M. Doporto, A. J. Fisher, T. J. B. M. Janssen, J. A. A. J. Perenboom, M. Kurmoo, W. Hayes, and P. Day, Phys. Rev. B **45**, 13 904 (1992).
[25] T. Sasaki and N. Toyota, Phys. Rev. B **48**, 11 457 (1993).
[26] J. S. Brooks, C. C. Agosta, S. J. Klepper, M. Tokumoto, N. Kinoshita, H. Anzai, S. Uji, H. Aoki, A. S. Perel, G. J. Athas, and D. A. Howe, Phys. Rev. Lett. **69**, 156 (1992).
[27] For a text, T. Ishiguro and K. Yamaji, *Organic Superconductors* (Springer-Verlag, Berlin, 1990).
[28] T. Osada, S. Kagoshima, and N. Miura, Synth. Met. **70**, 931 (1995).
[29] K. Kishigi and K. Machida, J. Phys. Soc. Jpn. **64**, 3853 (1995).
[30] P. Christ, W. Biberacher, H. Müller, K. Andres, E. Steep, and A. G. M. Jansen, Physica B **204**, 153 (1995); P. Christ, W. Biberacher, H. Müller, and K. Andres, Solid State Commun. **91**, 451 (1994).
[31] T. Sasaki, T. Fukase, and N. Toyota, Physica B **216**, 366 (1996).
[32] K. Mortensen, Y. Tomkiewicz, and K. Bechgaard, Phys. Rev. B **25**, 3319 (1982).
[33] T. Ando, A. B. Fowler, and F. Sterm, Rev. Mod. Phys. **54**, 437 (1982).
[34] G. M. Yin and K. Maki, Phys. Rev. B **44**, 7085 (1991).
[35] D. Shoenberg, *Magnetic Oscillations in Metals* (Cambridge University Press, Cambridge, 1984).
[36] T. Sasaki and N. Toyota, Synth. Met. **55-57**, 2296 (1993).
[37] T. Sasaki, H. Sato, and N. Toyota, Solid State Commun. **76**, 507 (1990).
[38] J. Caulfield, W. Lubczynski, F. L. Pratt, J. Singleton, D. Y. K. Ko, W. Hays, M. Kurmoo, and P. Day, J. Phys. Condens. Matter **6**, 2911 (1994).
[39] G. J. Athas, J. S. Brooks, S. Valfells, S. J. Klepper, M. Tokumoto, N. Kinoshita, T. Kinoshita, and Y. Tanaka, Phys. Rev. B **50**, 17 713 (1994).
[40] L. P. Gor'kov and A. G. Lebed, J. Phys. (France) Lett. **45**, L-433 (1984).
[41] P. M. Chaikin, Phys. Rev. B **31**, 4770 (1985).
[42] M. Heritier, G. Montambaux, and P. Lederer, J. Phys. (France) Lett. **45**, L-943 (1984).
[43] G. Montambaux, Phys. Rev. B **38**, 4788 (1988).
[44] G. M. Danner, P. M. Chaikin, and S. T. Hannahs, Phys. Rev. B **53**, 2727 (1996).
[45] I. S. Gradshteyn and I. M. Ryzhik, *Tables of Integrals, Series, and Products* (Academic Press, London, 1980).
[46] A. G. Lebed (unpublished).